

Supporting Information for
Peptide Self-Assembled Nanostructures with Distinct Morphologies
and Properties Fabricated by Molecular Design

Meiwen Cao,^{*[a](#)} Sha Lu,^a Wenjing Zhao,^a Li Deng,^a Meng Wang,^a Jiqian Wang,^a Peng Zhou,^a Dong Wang,^a Hai Xu,^{*[a](#)} Jian R. Lu^{[*,b](#)}

^a State Key Laboratory of Heavy Oil Processing and Centre for Bioengineering and Biotechnology, China University of Petroleum (East China), 66 Changjiang West Road, Qingdao 266580, China

^b Biological Physics Laboratory, School of Physics and Astronomy, University of Manchester, Schuster Building, Oxford Road, Manchester M13 9PL, United Kingdom

Corresponding Authors

* E-mail: mwcao@upc.edu.cn (M.W.C); xuh@upc.edu.cn (H.X.);
j.lu@manchester.ac.uk (J.R.L)

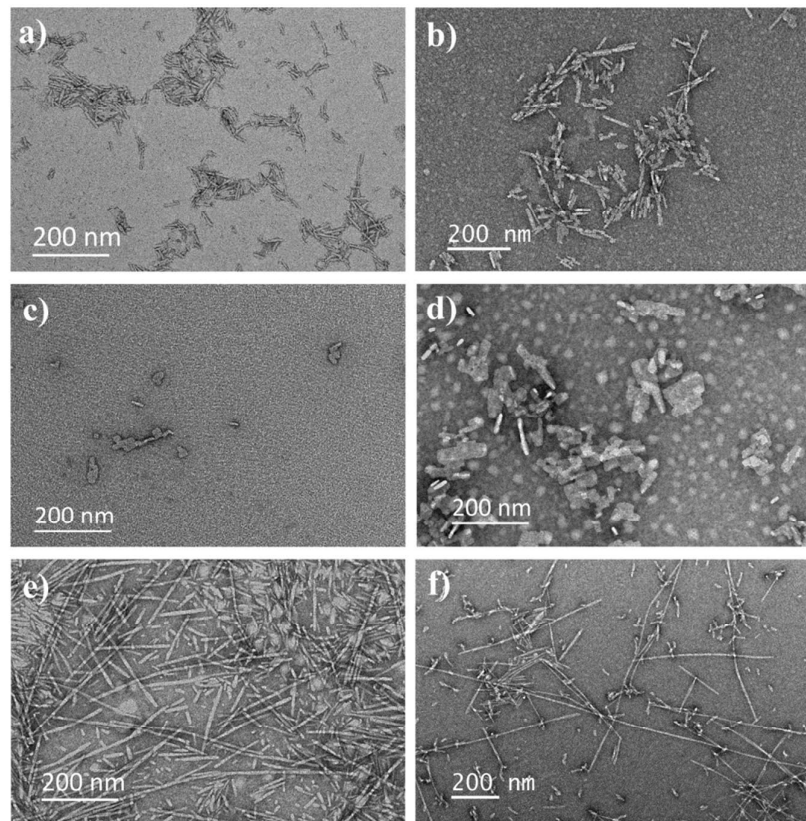


Figure S1. TEM images showing the self-assembled structures of (a) $\text{G}_3\text{A}_3\text{V}_3\text{I}_3\text{K}_3$, (b) $\text{K}_3\text{I}_3\text{V}_3\text{A}_3\text{G}_3$, (c) $\text{I}_3\text{V}_3\text{A}_3\text{G}_3\text{K}_3$, (d) $\text{K}_3\text{G}_3\text{A}_3\text{V}_3\text{I}_3$, (e) $\text{V}_3\text{G}_3\text{I}_3\text{A}_3\text{K}_3$, and (f) $\text{K}_3\text{A}_3\text{I}_3\text{G}_3\text{V}_3$ at 1.0 mM (just above their CACs) and pH 4.0 ± 0.5 .

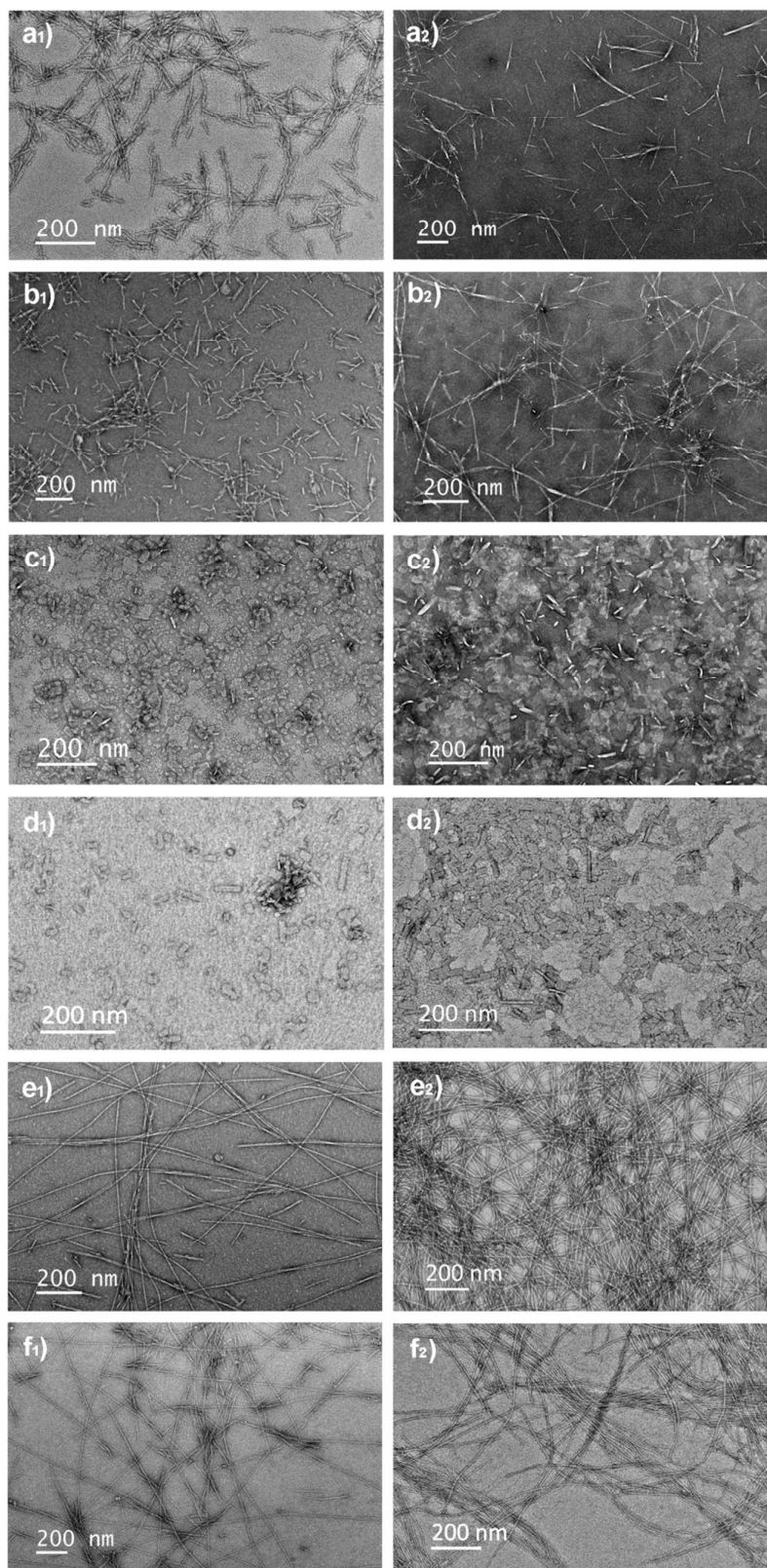


Figure S2. TEM images showing the self-assembled structures of (a) $K_3I_3V_3A_3G_3$, (b)

$\text{G}_3\text{A}_3\text{V}_3\text{I}_3\text{K}_3$, (c) $\text{K}_3\text{G}_3\text{A}_3\text{V}_3\text{I}_3$, (d) $\text{I}_3\text{V}_3\text{A}_3\text{G}_3\text{K}_3$, (e) $\text{K}_3\text{A}_3\text{I}_3\text{G}_3\text{V}_3$, and (f) $\text{V}_3\text{G}_3\text{I}_3\text{A}_3\text{K}_3$ at 4.0 mM (well above their CACs) and pH of either 7.0 ± 0.5 (left panel) or 10.0 ± 0.5 (right panel).

Table S1. The best-fitted structural parameters for the SANS data as shown in Figure 4.

Peptide	$\text{G}_3\text{A}_3\text{V}_3\text{I}_3\text{K}_3$	$\text{K}_3\text{I}_3\text{V}_3\text{A}_3\text{G}_3$	$\text{I}_3\text{V}_3\text{A}_3\text{G}_3\text{K}_3$	$\text{K}_3\text{G}_3\text{A}_3\text{V}_3\text{I}_3$	$\text{V}_3\text{G}_3\text{I}_3\text{A}_3\text{K}_3$
Fitting models	FlexCylEllipX Model		Lamellar Model + Elliptical Cylinder Model		Flexible Cylinder Model
Fitting parameters	axis_ratio	0.59	0.50	—	—
	kuhn_length	182Å	190Å	—	375Å
	Length	264Å	255Å	—	>1000Å
	Radius	33Å	39Å	—	24Å
	p1_length	—	—	264Å	192Å
	p1_r_minor	—	—	24Å	20Å
	p1_r_ratio	—	—	2.89	1.62
	p1_scale	0.024	0.052	0.013	4.1×10^{-3}
	p1_sldCyl	3.08×10^6	3.61×10^6	3.58×10^6	3.58×10^6
	p1_sldSolv	6.35×10^6	6.35×10^6	6.35×10^6	6.35×10^6
	p2_bi_thick	—	—	48Å	41Å
	p2_scale	—	—	1.5×10^{-3}	0.067
	p2_sld_bi	—	—	3.58×10^6	3.58×10^6
	p2_sld_sol	—	—	6.35×10^6	6.35×10^6
	scale_factor	—	—	0.81	0.11

The models used for fitting the small angle neutron scattering (SANS) data are detailed as follows.

(1) The Lamellar Model:

The fundamental theory of the lamellar model can be found from reference [Nallet et al, *J. Phys. II France* **1993**, 3, 487]¹.

In the fitting parameters, sld.bi = the scattering length density (SLD) of the bilayer,

sld_sol = SLD of the solvent, and bi_thick = the thickness of the bilayer.

(2) The Flexible Cylinder Model:

The fundamental theory of the flexible cylinder model can be found from references [Pedersen et.al, *Macromolecules* **1996**, *29*, 7602]² and [Chen et. al, *Langmuir* **2006**, *22*, 6539]³.

In this model, the chain of contour length can be described as a chain of some number of locally stiff segments of length L_p (L_p : the persistence length, the length along the chain over which the flexible cylinder can be considered as a rigid rod). The Kuhn length = $2 \times L_p$. In the fitting parameters, the sldCyl and sldSolv represent SLD (chain/cylinder) and SLD (solvent), respectively.

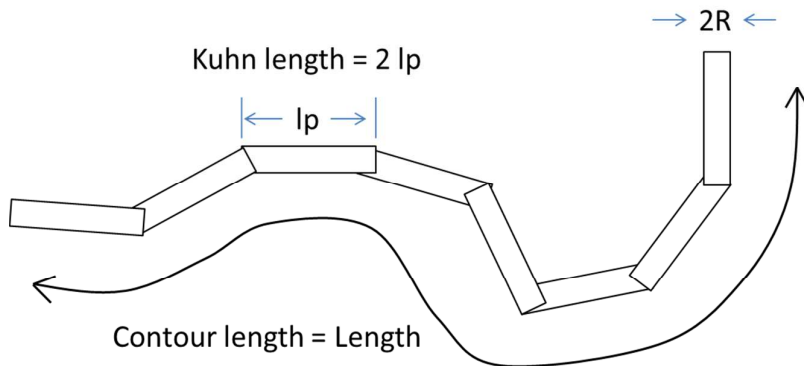


Figure S3. Scheme for the Flexible Cylinder Model.

(3) The FlexCylEllipX Model:

The fundamental theory of the FlexCylEllipX Model can be found from references [Pedersen et.al, *Macromolecules* **1996**, *29*, 7602]² and [Chen et. al, *Langmuir* **2006**, *22*, 6539]³.

Basically the FlexCylEllipX Model takes the same theory as that of the flexible cylinder model. However, the cross section of the cylinder is elliptical, with a minor

radius and a major radius. Therefore, the axis ratio is greater than one. This inequality should be maintained by following simple constraints in curve fitting.

(4) The Elliptical Cylinder Model:

The fundamental theory of the elliptical cylinder model can be found from reference [Feigin et. al, “Structure Analysis by Small-Angle X-Ray and Neutron Scattering”, Plenum, New York, 1987]⁴.

This model calculates the scattering from an oriented elliptical cylinder. In the fitting parameters, the sldCyl and sldSolv represent SLD (chain/cylinder) and SLD (solvent), respectively.

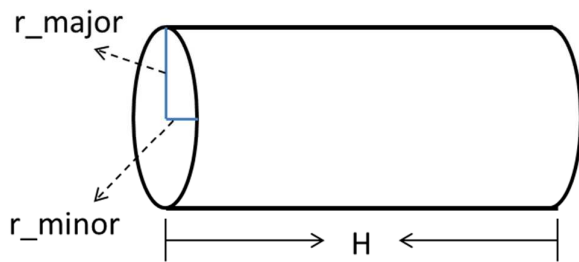


Figure S4. Scheme for the Elliptical Cylinder Model. In this model, $r_{ratio} = r_{major}/r_{minor}$.

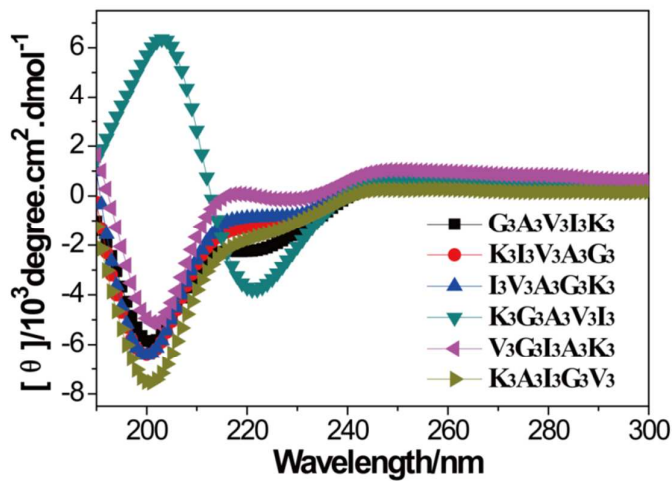


Figure S5. CD spectra of the peptides at 0.5 mM and pH 4.0 ± 0.2.

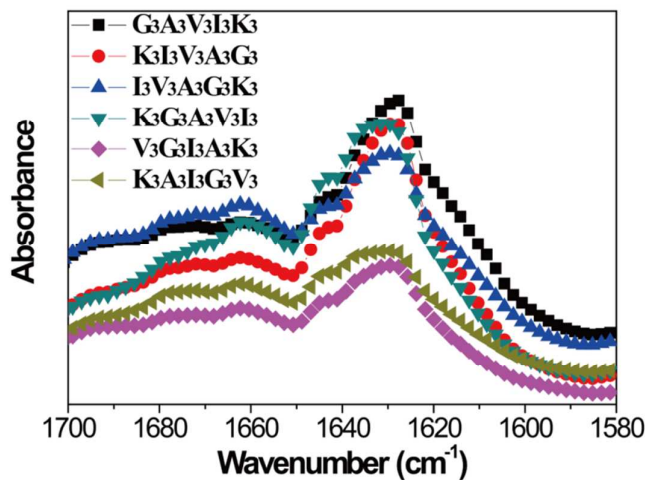


Figure S6. ATR-FTIR spectra of the peptides at 4.0 mM and pH 4.0 ± 0.2.

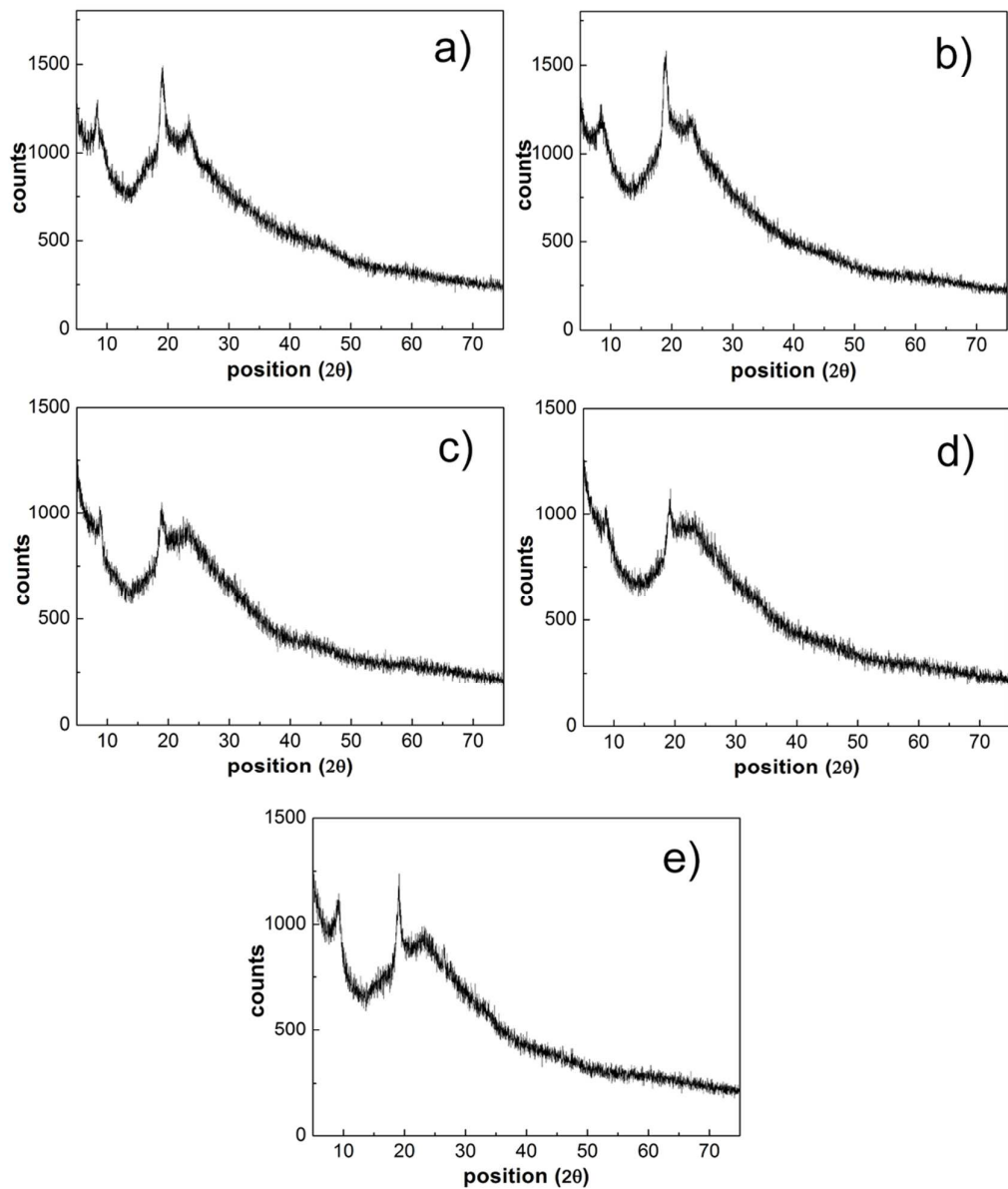


Figure S7. XRD spectra of (a) G₃A₃V₃I₃K₃, (b) K₃I₃V₃A₃G₃, (c) V₃G₃I₃A₃K₃, (d) K₃A₃I₃G₃V₃, and (e) K₃G₃A₃V₃I₃ powders obtained from freeze-drying of 16.0 mM peptide solutions.

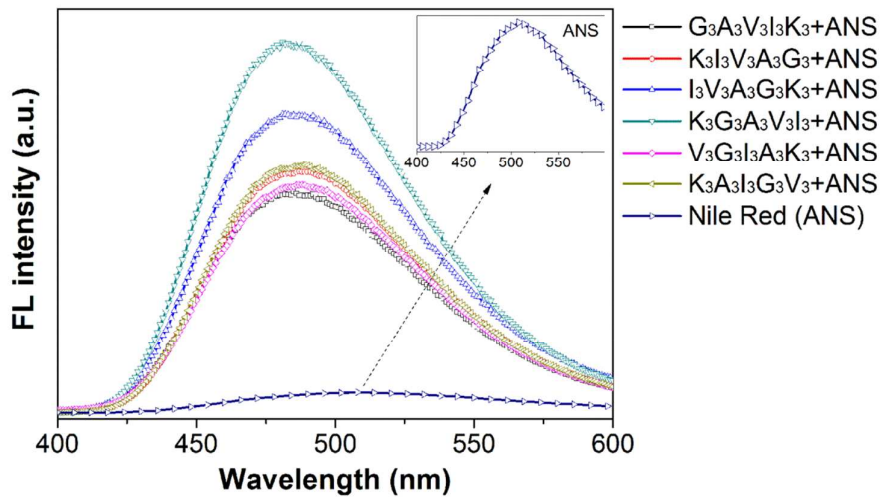


Figure S8. Fluorescence spectra of the 8-anilino-1-naphthalenesulfonate (ANS) itself and the ANS encapsulated in the peptide nanostructures. The peak wavelength of ANS works well in detecting the internal polarity of peptide nanostructures.^{5,6} ANS in water gave fluorescence spectrum peaked at 511 nm. When dissolved in peptide solutions, the ANS peak showed significant blue shifts to 480–490 nm. Based on the peak wavelength of ANS, a normalized polarity scale, E_T^N , can be obtained, which works well in detecting the internal polarity of peptide nanostructures.⁶

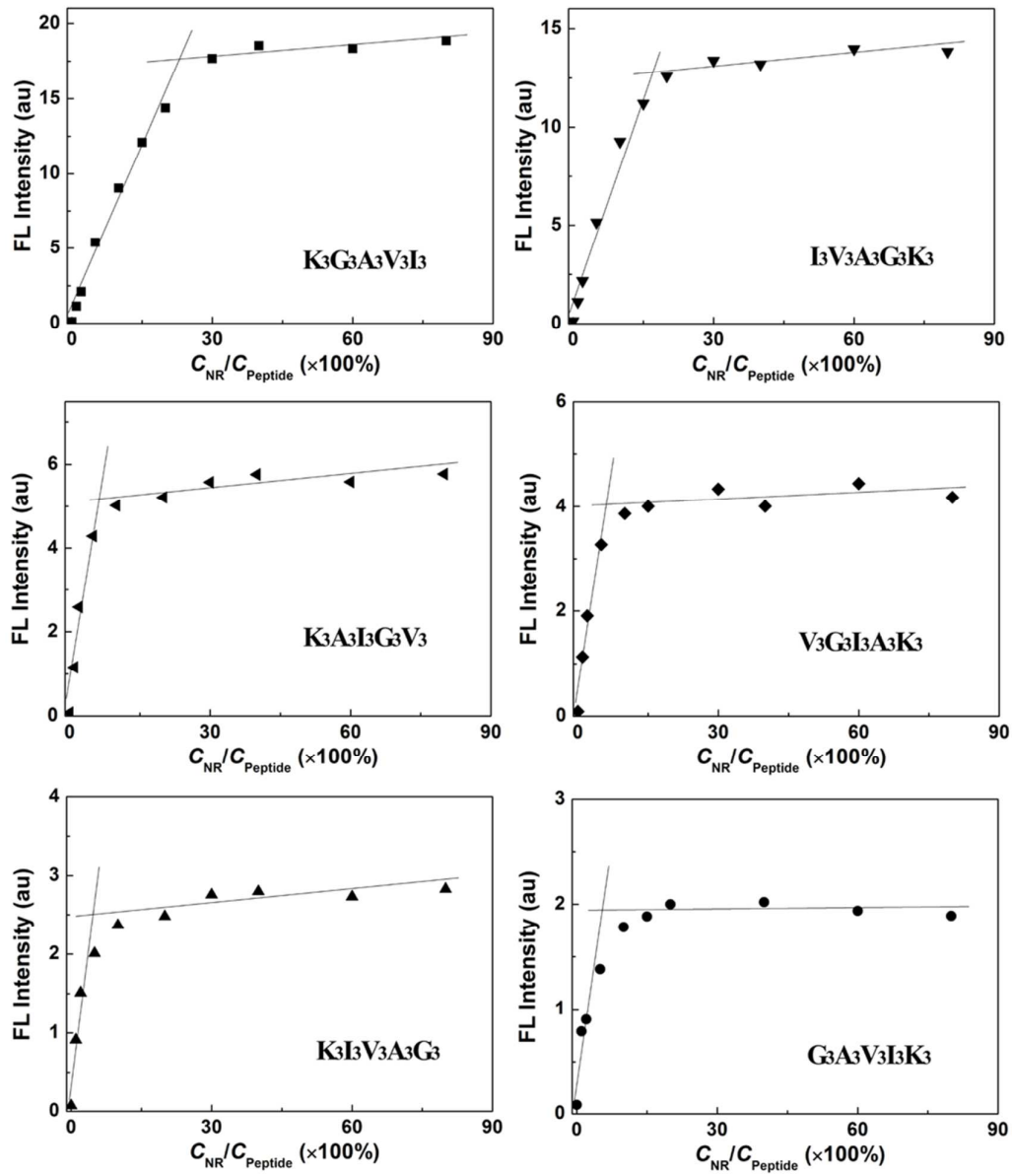


Figure S9. Determination of Nile red (NR) encapsulation efficiency by the fluorescence method. The fluorescence intensity is plotted as a function of the molar ratio of NR to peptide. The saturation point of encapsulation was determined by the intercept of two linear fits extrapolating the data points from below and above the region in which a rapid change of slope was observed.

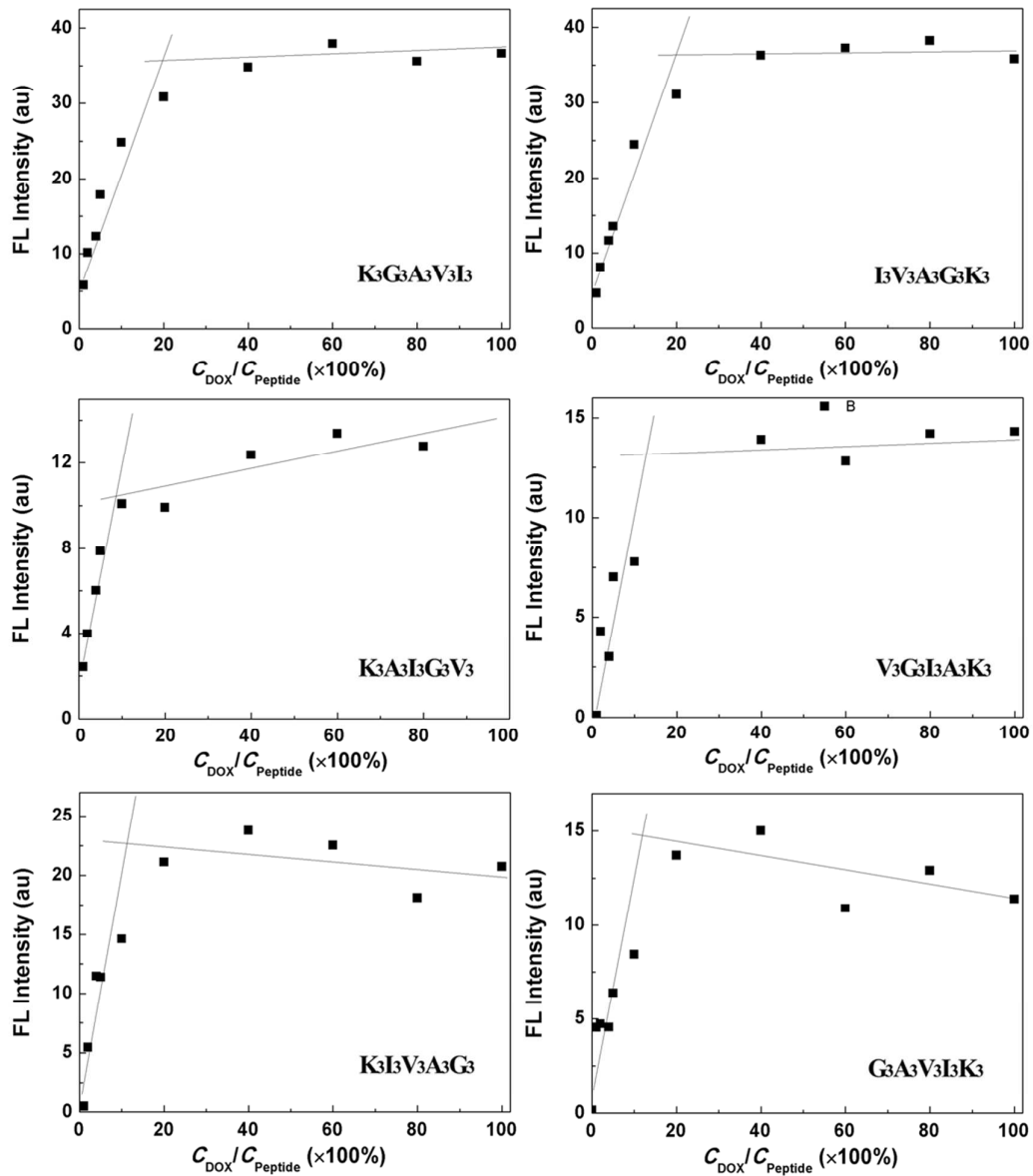


Figure S10. Determination of doxorubicin (DOX) encapsulation efficiency by the fluorescence method.

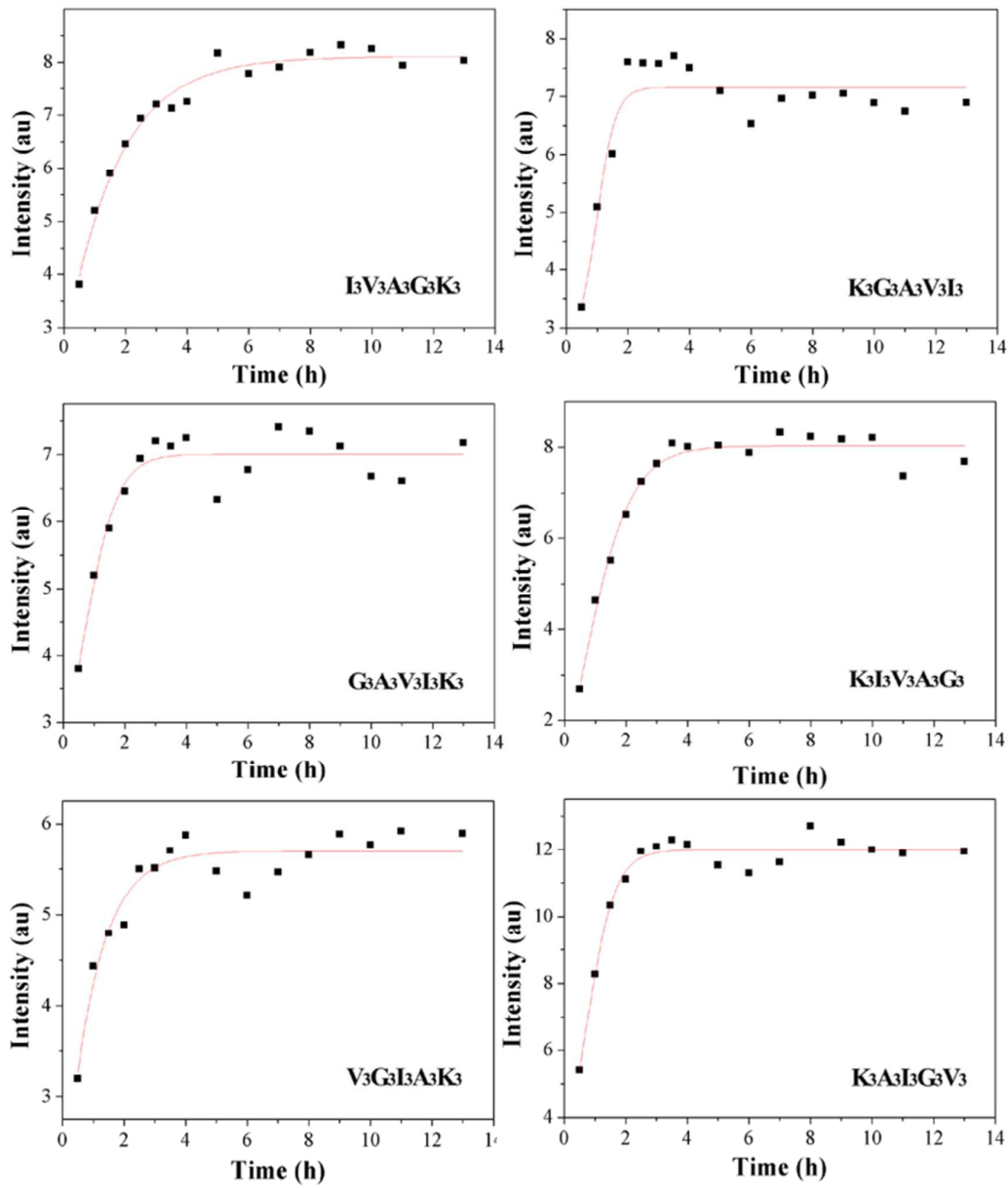


Figure S11. Determination of DOX release from the DOX-loaded peptide nanostructures. The fluorescence intensity of the dialyzate was plotted as a function of incubation time.

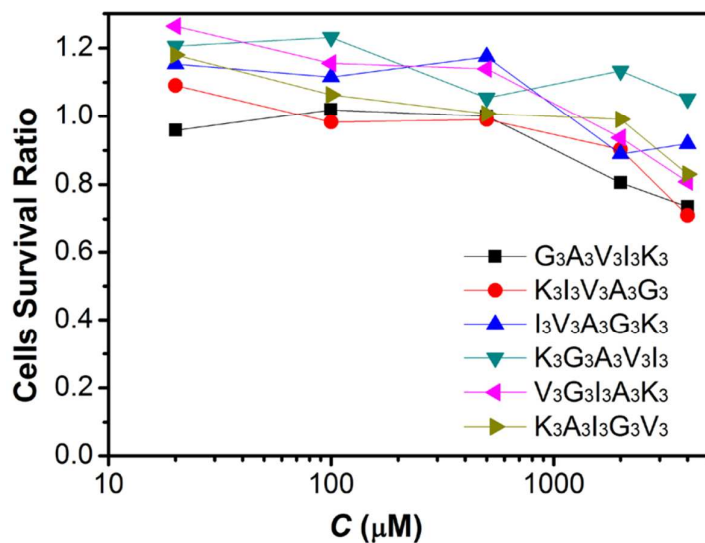


Figure S12. Cytotoxicity of different peptides towards HeLa cells as determined by the MTT assay.

References:

- (1) Nallet, F.; Laversanne, R.; Roux, D. *J. Phys. II France* **1993**, *3*, 487.
- (2) Pedersen, J. S.; Schurtenberger, P. *Macromolecules* **1996**, *29*, 7602.
- (3) Chen, W.-R.; Butler, P. D.; Magid, L. J. *Langmuir* **2006**, *22*, 6539.
- (4) Feigin, L.; Svergun, D. I. *Structure analysis by small-angle X-ray and neutron scattering*; Springer, 1987.
- (5) Hayashida, O.; Ono, K.; Hisaeda, Y.; Murakami, Y. *Tetrahedron* **1995**, *51*, 8423.
- (6) Shao, H.; Parquette, J. R. *Angew Chem Int Ed Engl* **2009**, *48*, 2525.